ACS APPLIED MATERIALS & INTERFACES

Research Article

www.acsami.org

Effects of Carbon and Nitrogen Plasma Immersion Ion Implantation on In vitro and In vivo Biocompatibility of Titanium Alloy

Ying Zhao,[†,‡] Sze Man Wong,[†] Hoi Man Wong,[†] Shuilin Wu,[‡] Tao Hu,[‡] Kelvin W. K. Yeung,*[,†] and Paul K. Chu*[,‡]

[†]Department of Orthopaedics & Traumatology, The University of Hong Kong, Pokfulam Road, Hong Kong, China

[‡]Department of Physics & Materials Science, City University of Hong Kong, Tat Chee Avenue, Kowloon, Hong Kong, China

Supporting Information

ABSTRACT: Growth of bony tissues on titanium biomedical implants can be time-consuming, thereby prolonging recovery and hospitalization after surgery and a method to improve and expedite tissue-implant integration and healing is thus of scientific and clinical interests. In this work, nitrogen and carbon plasma immersion ion implantation (N−PIII and C−PIII) is conducted to modify Ti-6Al-4V to produce a graded surface layer composed of TiN and TiC, respectively. Both PIII processes do not significantly alter the surface hydrophilicity but increase the surface roughness and corrosion resistance. In vitro studies disclose improved cell adhesion and proliferation of MC3T3-E1 preosteoblasts and L929 fibroblasts after PIII. Micro-CT evaluation conducted 1 to 12 weeks after surgery reveals larger average bone volumes and less bone resorption on the N−PIII and C−PIII titanium alloy pins than the unimplanted one at every time point. The enhancements observed from both the in vitro and in vivo studies can be attributed to the good cytocompatibility, roughness, and corrosion resistance of the TiN and TiC structures which stimulate the response of preosteoblasts and fibroblasts and induce early bone formation. Comparing the two PIII processes, N−PIII is more effective and our results suggest a simple and practical means to improve the surface biocompatibility of medical-grade titanium alloy implants.

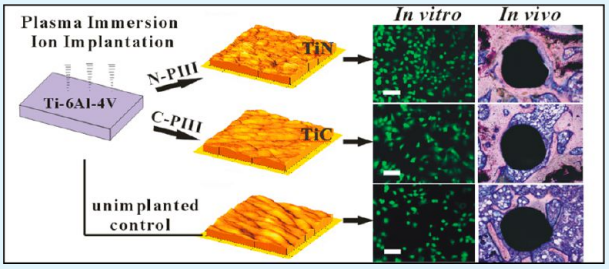

KEYWORDS: *titanium alloys, plasma immersion ion implantation, cytocompatibility, surface chemistry, cells, bones*

1. INTRODUCTION

Ti-6Al-4V alloy is widely used in joint prostheses and fracture fixation devices because of the good mechanical properties and excellent corrosion resistance. However, long-term success of orthopedic implants made of Ti-6Al-4V still needs to be addressed because of inherent bioinertness and insufficient osseointegration.[1,2] Faster healing at the bone−implant interface not only improves the implant stability and longevity but also shortens hospitalization.[3] Surface modification is a viable strategy to improve implant integration with bones and accelerate healing, and among the various techniques, plasma-based surface modification is versatile and attractive because selected biomedical and surface properties such as corrosion resistance and cytocompatibility can be enhanced whereas the favorable attributes of the bulk materials such as hardness and strength can usually be preserved.[4−7] In particular, plasma immersion ion implantation (PIII) circumvents the line-of-sight restriction in conventional beamline ion implantation and is especially suitable for biomedical implants with a complex geometry.[8] For example, nitrogen and carbon PIII has been conducted to improve the surface hardness and wear resistance of Ti-6Al-4V.[9−12] However, a comprehensive evaluation of the effects of carbon PIII (C−PIII) and nitrogen PIII (N−PIII) on the preosteoblast and fibroblast response in vitro and new bone formation on Ti-6Al-4V in vivo has not been conducted. The objectives of this work are to conduct the systematic investigation, correlate the various surface characteristics with cytocompatibility and bone growth in vitro and in vivo, and elucidate the underlying mechanisms.

2. MATERIALS AND METHODS

2.1. Specimen Preparation and Modification. Medical grade Ti-6Al-4V alloy samples purchased from Goodfellow, Cambridge Limited, UK ($\Phi 5 \times 2$ mm^2 and $\Phi 14 \times 2$ mm^2) were ground with SiC paper progressively up to 1200 grits and then mechanically polished to a mirror finish with 1 μm diamond paste. Afterward, the samples were ultrasonically washed in acetone and ethanol and dried prior to PIII. C−PIII was conducted on a multipurpose plasma immersion ion implanter equipped with a graphite cathodic arc source in the Plasma Laboratory in City University of Hong Kong for 2 h using pulsed voltage, pulse duration, and pulsing frequency of −30 kV, 500 μs, and 10 Hz, respectively.[13,14] During C−PIII, Ar was bled into the chamber at a flow rate of 4 standard cubic centimeters per minute (sccm) and the carbon plasma was created by vacuum arc discharge. N−PIII was conducted on the GPI-100 ion implanter. The nitrogen plasma was formed in the chamber using a nitrogen flow rate of 20 sccm. Using

Received: December 12, 2012
Accepted: January 31, 2013
Published: January 31, 2013

pulsed voltage, pulse width, and pulsing frequency of −30 kV, 30 μs, and 100 Hz, respectively, N−PIII was conducted for 2 h.

2.2. Surface Characterization. To determine the surface chemical composition and elemental depth profiles, X-ray photoelectron spectroscopy (XPS) was conducted on a Physical Electronics PHI 5802 equipped with a monochromatic Al K_α source. The sputtering rate was estimated to be about 5.67 nm·min^{-1} based on that calculated from a SiO_2 standard sputtered under similar conditions and the binding energies were referenced to the C 1s line at 285.0 eV. The Ti 2p spectra acquired after sputtering for 4 min were deconvoluted by Gaussian−Lorentzian peak fitting. The surface morphology was examined by atomic force microscopy (AFM) (Auto-Probe CP, Park Scientific Instruments) in the contact mode and the surface hydrophilicity of the samples was assessed by water contact angle measurements performed on a Ramé-Hart (USA) instrument at ambient humidity and temperature. The electrochemical polarization curves were acquired on a Zahner Zennium electrochemical workstation using the conventional three-electrode technique in simulated body fluids (SBF).[15] The potential was referenced to a saturated calomel electrode (SCE) with a platinum sheeting serving as the counter electrode. The samples with a surface area of 10 × 10 mm^2 were exposed to the SBF at 37 °C and the polarization curves were obtained at a scanning rate of 1 mV/s.

2.3. In vitro Studies. *2.3.1. Cell Culture.* Mouse MC3T3-E1 preosteoblasts and mouse L929 fibroblasts were employed to investigate the effects of PIII on the cell behavior. All the cells were cultivated in a complete cell culture medium consisting of a mixture of Dulbecco's modified eagle medium (DMEM, Gibco) and 10% bovine serum (FBS, Gibco) in a humidified atmosphere of CO_2 at 37 °C.

2.3.2. Initial Cell Adhesion. Prior to cell cultivation, the samples were sterilized by immersing in 75% (v/v) ethanol for 30 min and subsequently rinsed three times with sterile phosphate buffered saline (PBS). The MC3T3-E1 preosteoblasts and L929 fibroblasts were seeded on each sample in 96 well tissue culture plates at a density of 1 × 10^4 cells per well and cultured for 4 h. Afterward, the seeded samples were rinsed twice with sterile PBS, fixed with 2% polyoxymethylene solution, and stained with the aid of LIVE/DEAD Staining Kit sequentially. The number of cells is determined from three random fields using a fluorescence microscope (Carl Zeiss Axioplan 2).

2.3.3. Cell Proliferation Assay. The MTT assay was used to determine the cell viability and cell proliferation. MC3T3-E1 preosteoblasts and L929 fibroblasts were seeded at a density of 5 × 10^3 cells/well on the samples in 96-well tissue culture plates and cultured for 2, 4, or 7 days. At the end of the incubation period, the samples were rinsed twice with sterile PBS and transferred to a fresh 96-well tissue culture plate. The attached cells were incubated in DMEM containing 5 mg/mL of thiazolyl blue tetrazolium bromide (MTT, Sigma) for 4 h. After carefully removing the medium, the purple formazan product was dissolved in dimethyl sulfoxide and the optical density (OD) values were recorded by a PowerWave Microplate Spectrophotometer (BioTek, USA) at 570 nm wavelength to determine the cell viability. The results of the in vitro cell experiments were statistically analyzed using one-way analysis of variance (ANOVA) and a p value of less than 0.05 was considered to indicate statistical significance.

2.4. In vivo Animal Study. *2.4.1. Surgery.* Twelve-week-old male ICR rats were used as the animal model. They were housed at 18−22 °C and relative humidity of 55−70% at the Laboratory Animal Unit of The University of Hong Kong. Prior to surgery, all the rats were anaesthetized with hypnorm (12.5 mg/kg) and dormicum (6.25 mg/kg). A hole 1.25 mm in diameter was prepared in the distal femurs using a dental drill until the hole reached 4 mm in depth. The Ti alloy pin (Φ1.5 × 4 mm^3) was implanted into the prepared holes on the left or right femur (Figure 1). Oxytetracycline (30 mg/kg) and ketoprofen (3 mg/kg) were administered postoperatively for 4 consecutive days. The protocol was approved by the University Ethics Committee and the Department of Health of The University of Hong Kong.

2.4.2. Bone Volume and Histological Evaluation. After surgery, the rats underwent microcomputed tomography (micro-CT) evaluation directly using a microcomputed tomography device (SKYSCAN 1076, Skyscan Company) and more micro-CT examination was conducted every week up to the 12th week. After scanning, the 2D planes were reconstructed using NRecon (Skyscan Company) and the 3D models were generated by CTVol (Skyscan Company). The bone volume around the implant was analyzed by the CTAn program (Skyscan Company) which was also used to examine the micro-CT data sets for new bone growth.

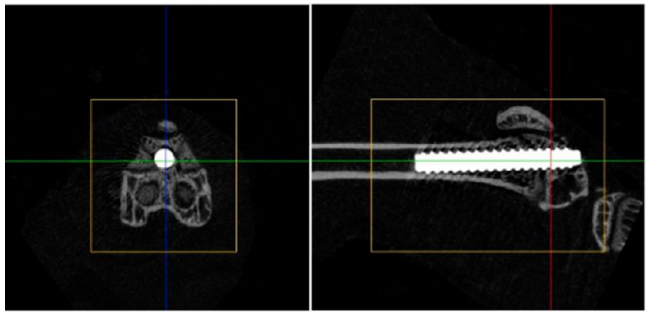

Figure 1. Micro-CT image of femur after implantation of Ti alloy pin: (a) top view and (b) side view.

The bone samples with implants were harvested 12 weeks after surgery and fixed in 10% buffered formalin for 3 days, dehydrated in a series of solutions with different ethanol concentrations of 70, 80, 90, 99, and 100% v/v for 3 days each, and transferred to a methylmethacrylate (Technovit 9100 New, Heraeus Kulzer, Hanau, Germany) solution at 37 °C within 1 week. Afterward, the embedded samples were cut into sections with a thickness of 50−70 mm. The sectioned samples were stained with gimesa and eosin (MERCK, Germany) stain and the morphological and histological analyses were performed using an optical microscope.

3. RESULTS

3.1. Characterization of Samples. The XPS depth profiles and high-resolution XPS Ti 2p, C1s, and N1s spectra acquired from the C−PIII and N−PIII samples are depicted in Figure 2. A C-rich graded layer about 340 nm (sputtering 60 min) thick is found on the C−PIII sample. After sputtering for 4 min to remove the surface materials such as those stemming from carbon and oxygen adsorption, the high-resolution XPS Ti 2p3/2 spectrum is acquired showing that the outer layer is composed of TiC, TiO_2, Ti_2O_3, TiO, and Ti corresponding to binding energies of 454.9, 458.9, 456.9, 455.1, and 454.3 eV, respectively, according to Gaussian−Lorentzian peak fitting.[16,17] With increasing sputtering time, the Ti 2p peak shifts to a lower binding energy, indicating that the amounts of oxide and carbide decrease gradually while the metallic states become more dominant. As a result of the non-UHV (ultrahigh vacuum) implantation conditions in our PIII instrument leading to unintentional surface oxidation,[18] the oxygen concentration decreases with depth but that of carbon shows an initial increase before diminishing typical of an ion implant distribution.

A stable N-rich layer is found on the N−PIII sample. The high-resolution XPS Ti 2p spectrum shows that the outer layer is composed of TiN (Ti 2p3/2 455.8 eV; N 1s 396.9 eV), TiO_2, Ti_2O_3, TiO, and Ti. The valence state of Ti gradually changes from the oxidized or nitrided state to the metallic one with sputtering. The implanted N exhibits a Gaussian-like distribution with a peak concentration of about 38 at %. The data show that the surface N concentration on the N−PIII sample is higher than the surface C concentration on the C−

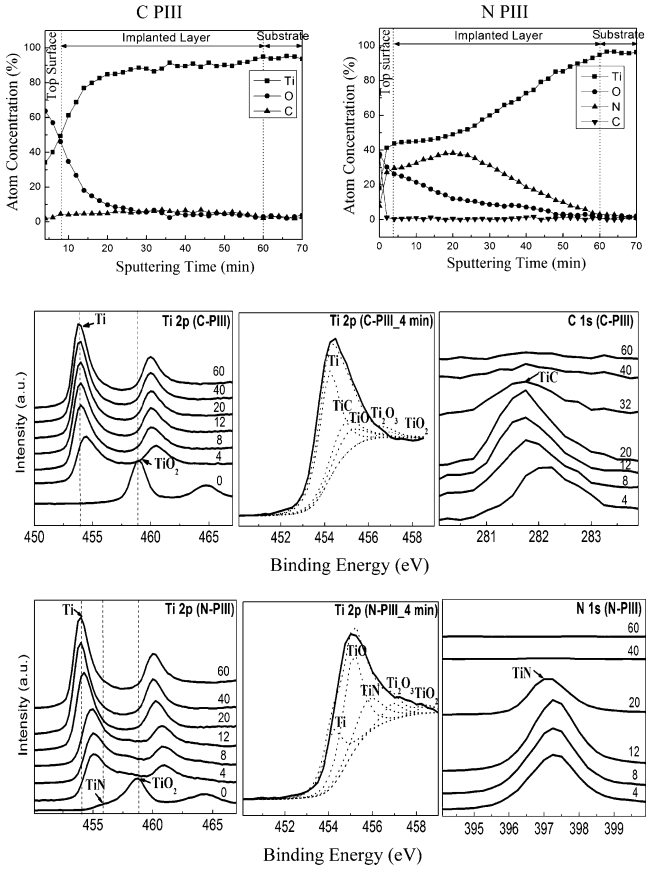

Figure 2. XPS depth profile and high-resolution XPS spectra acquired from the C−PIII and N−PIII Ti alloys at different sputtering time with the numbers in the figures denoting the sputtering time.

PIII sample, suggesting that N−PIII is more effective in forming the TiN surface structure than C−PIII forming TiC. It may be because the gas discharge efficiency of the radio frequency source (for N) is higher than that of the pulsed cathodic arc source (for C). When the sputtered depth reaches about 340 nm (sputtering 60 min), neither nitride nor oxide can be observed and the metallic state predominates.

The 3D AFM images acquired from a scanned range of 1 × 1 μm^2 are shown in Figure 3. The relatively smooth topography of the unimplanted sample (Figure 3a) is altered by PIII and nanosized pot-holes can be observed from the C−PIII and N−PIII surfaces (Figures 3b, c). The root-mean-square (RMS) surface roughness values increase from 1.15 nm on the unimplanted sample to 1.70 nm on the C−PIII sample and 2.33 nm on the N−PIII sample. A rough surface morphology usually bodes well for cell attachment.[19] The measured water contact angles are summarized as a histogram in Figure 4 furnishing evidence that PIII does not significantly alter the surface hydrophilicity of the Ti alloy and there is also no significant statistical difference between the C−PIII and N−PIII samples.

Figure 5 displays the representative potentiodynamic polarization curves before and after PIII acquired in SBF. The anodic breakdown potential (E_b) and anodic passive region (E_b−E_{corr}) of the three samples reveal significant differences. The N−PIII sample exhibits the highest anodic breakdown potential and largest anodic passive region, followed by the C−PIII sample with the unimplanted sample showing the least. The higher anodic breakdown potential and larger anodic passive region

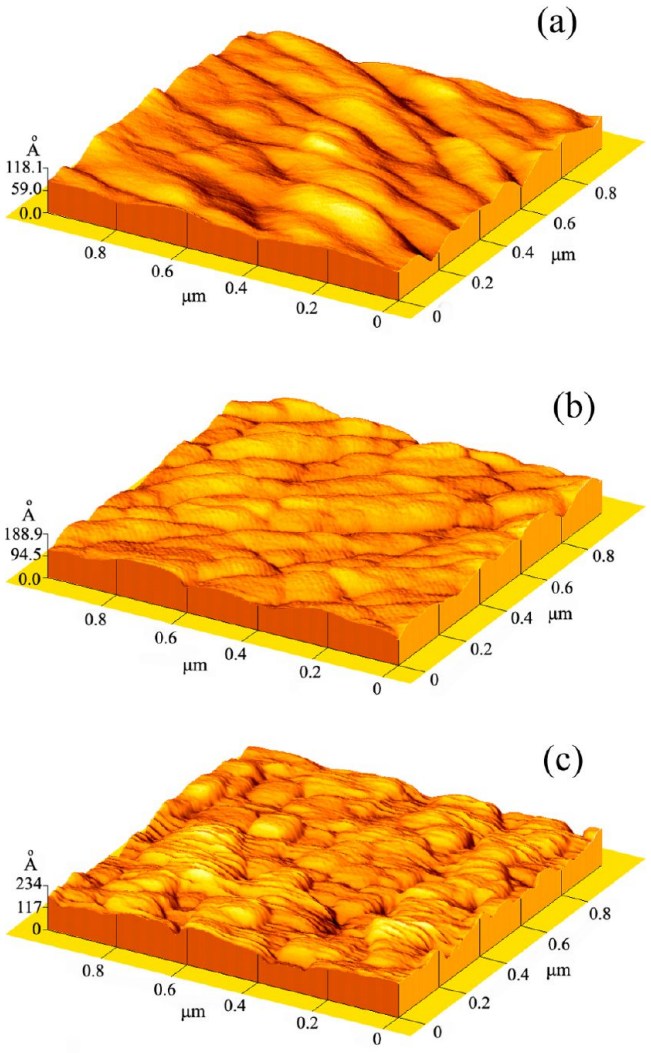

Figure 3. AFM images: (a) unimplanted Ti alloy, (b) C−PIII Ti alloy, and (c) N−III Ti alloy.

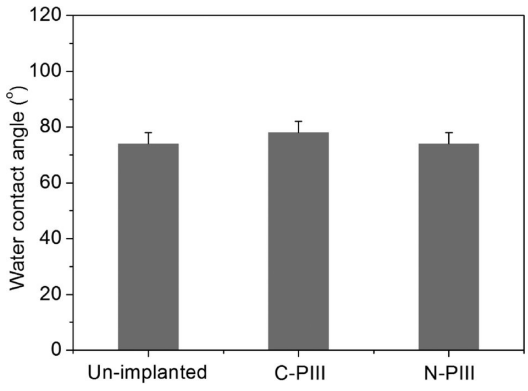

Figure 4. Water contact angles measured from the unimplanted, C−PIII and N−PIII samples.

correlate with better corrosion resistance and our results disclose that N−PIII give rise to the best corrosion resistance.

3.2. Cell Adhesion. The adhesion of MC3T3-E1 preosteoblasts and L929 fibroblasts on the unimplanted, C−PIII, and N−PIII samples is determined by fluorescence microscopy and the histograms are presented in Figure 6. Even

dx.doi.org/10.1021/am302961h | ACS Appl. Mater. Interfaces 2013, 5, 1510−1516

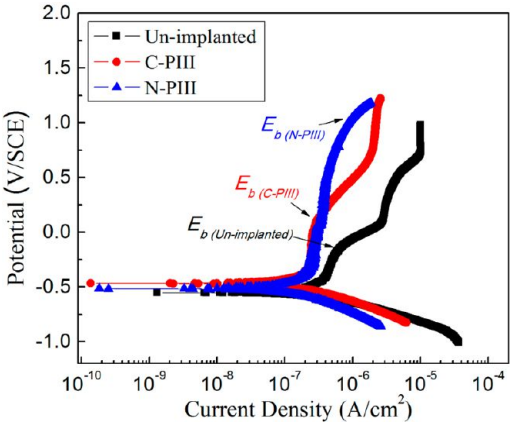

Figure 5. Polarization curves of the unimplanted, C−PIII, and N−PIII samples in SBF.

though the exact cell morphology on the different samples cannot be discerned under fluorescence microscopy, the number of adhered preosteoblasts and fibroblasts on the plasma-treated samples is larger than that on the unimplanted control, suggesting that the cytocompatibility is enhanced by PIII.

3.4. Cell Proliferation. The proliferation and viability of preosteoblasts and fibroblasts cultured on the unimplanted, C−PIII, and N−PIII samples for 2, 4, and 7 days are determined by the MTT assay and the results are illustrated in Figure 7. The degree of proliferation of the preosteoblasts and fibroblasts is higher on the plasma-treated surfaces than the unimplanted control at each prescribed time point and the improvement on the N−PIII sample is especially prominent. The in vitro cell culture assay discloses that after N−PIII and C−PIII, no significant cytotoxicity and even better cytocompatibility are observed.

3.5. Micro-Computed Tomography Analysis. The bone behavior around the Ti alloy pins in the living ICR rats is

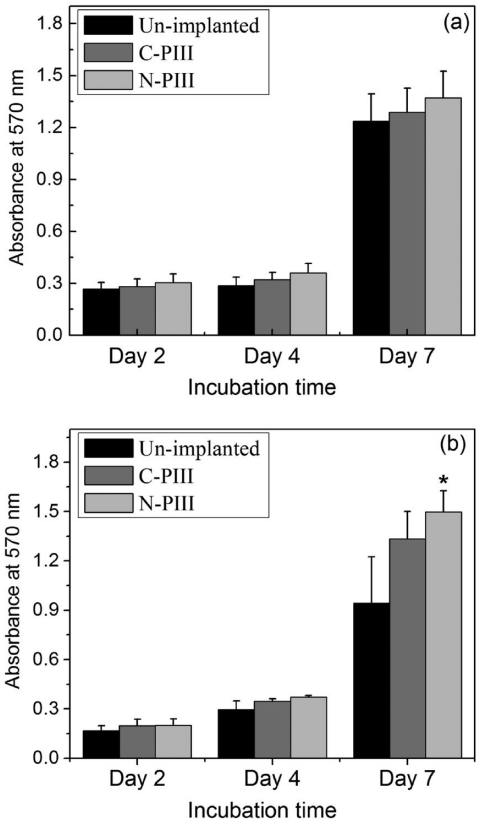

Figure 7. Cell proliferation assays: (a) osteoblasts and (b) fibroblasts cultured on the various samples for 2, 4, and 7 days. *p < 0.05 compared to the unimplanted control.

observed and evaluated by continuous micro-CT monitoring. Figure 8 shows the 2D and 3D micro-CT reconstruction images of the titanium alloy pins at 0, 1, 6, and 12 weeks after surgery and Figure 9 exhibits the corresponding change in the

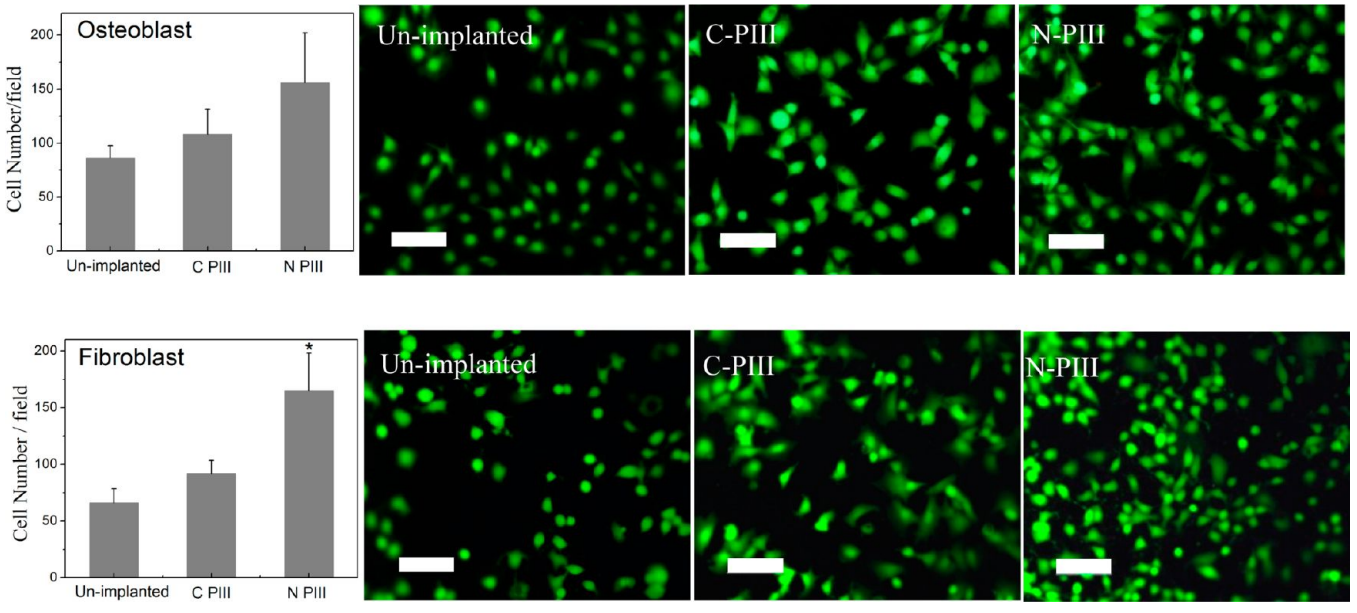

Figure 6. Adhesion of preosteoblasts (upper pictures) and fibroblasts (lower pictures) on the samples as determined by counting the cells stained with the LIVE/DEAD staining kit under a fluorescence microscope after incubation for 4 h. *p < 0.05 compared to the unimplanted control (scale bar is 200 μm).

dx.doi.org/10.1021/am302961h | ACS Appl. Mater. Interfaces 2013, 5, 1510−1516

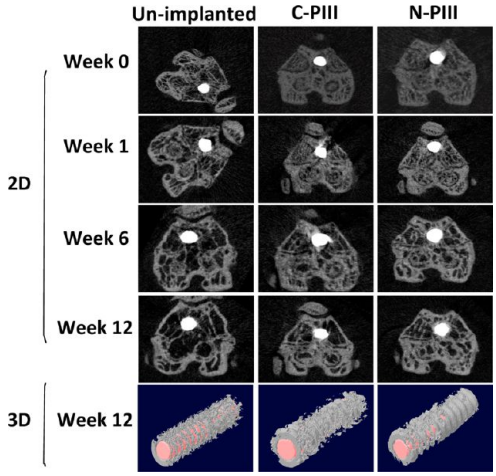

Figure 8. Micro-CT 2D and 3D reconstructions models showing the status of titanium alloy pins (bright white or pink in color) and bone (gray white in color) response 0, 1, 6, and 12 weeks after operation.

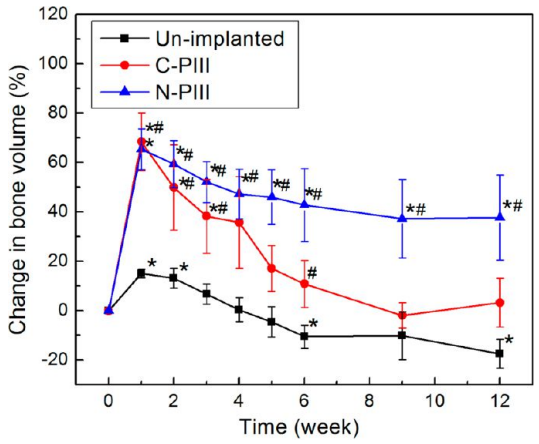

Figure 9. Changes in the bone volume around the Ti alloy pin after different implantation period (mean ± S.E.M., n = 4–12, * significantly different from time zero, # significantly different from the time-matched unimplanted control).

average bone volume from week 1 to week 12. During the whole implantation period, all the samples are stable and there is no apparent volume change. A closer examination reveals the largest average bone volume on the N–PIII Ti alloy pin, followed by that on the C–PIII sample with the unimplanted control faring the worst at every time point. Significantly enhanced bone volumes can be found on the C–PIII implant 2, 3, and 6 weeks after operation compared to the unimplanted control. In comparison, dramatically increased bone volumes can be observed from the N–PIII implant at all the prescribed time points compared to the unimplanted control. The in vivo study confirms that N–PIII induces the most favorable bone behavior.

Figure 9 shows that that the bone volumes on the Ti alloy pins are the largest one week after surgery and then decrease. Fracture healing in bone consists of several overlapping phases; inflammation, soft and hard callus formation, and remodeling.[20] In the first week after surgery, the tissues undergo the inflammatory phase, soft callus formation, as well as hard callus formation. Therefore, the hard tissue volume increases. However, after 1 week when the unorganized hard tissues undergo the bone remodelling phase, the bone reabsorbs and reorganizes itself thus resulting in a bone volume decrease. Our data suggest that PIII (in particular N–PIII) can effectively reduce bone resorption.

3.6. Histological Analysis. Figure 10 shows the tissue response on the unimplanted, C–PIII, and N–PIII Ti samples

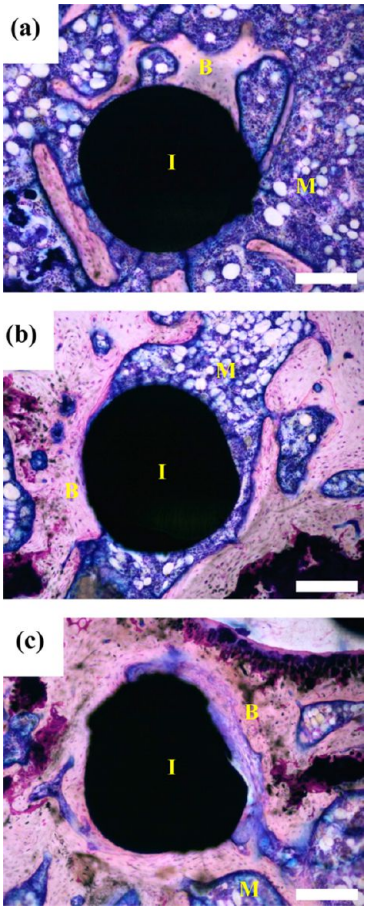

Figure 10. Hard tissue sections of Gimesa and Eosin stained around the implant after implantation for 12 weeks where "I" represents implant, "B" represents bone, and "M" represents bone marrow: (a) unimplanted Ti alloy, (b) C–PIII Ti alloy, and (c) N–PIII Ti alloy (scale bar is 200 μm).

12 weeks after implantation by means of gimesa and eosin staining. All the implants show direct contact with the newly formed bone. More bone is formed around the N–PIII implant than the C–PIII implant and unimplanted control.

4. DISCUSSION

A rough surface structure containing TiN or TiC is produced on the titanium alloy by N–PIII or C–PIII to induce more initial cell adhesion, proliferation, and new bone formation. It is well-known the biological response to biomaterials is largely controlled by their surface chemistry, morphology, and hydrophilicity. That is to say, the surface characteristics play a vital role in the functions of biomaterials[21,22] and so it is important to understand how N–PIII and C–PIII impact the surface characteristics of the Ti alloy. In PIII, the samples are surrounded by the overlying plasma and pulse-biased to a high negative potential. Energetic ion bombardment alters the surface morphology. As shown in the AFM results, the surface roughness increases significantly after PIII and the modified

dx.doi.org/10.1021/am302961h | ACS Appl. Mater. Interfaces 2013, 5, 1510–1516

surfaces are more compatible with preosteoblasts and fibroblasts. Good cell adhesion and proliferation can be achieved on rough surfaces[23,24] but decreased cell functions have also been reported on rough surfaces.[25,26] Therefore, the surface roughness may not be the dominant factor affecting in vitro cellular response and additional O−PIII is conducted here. Figure 2S in the Supporting Information exhibits the initial adhesion and proliferation of preosteoblasts and fibroblasts on the O−PIII sample as well as unimplanted control. The in vitro cell adhesion of the sample before and after O−PIII is in fact comparable. Cell proliferation on the O−PIII sample is slightly higher than that on the unimplanted control but inferior to that on the other N−PIII and C−PIII samples as shown in Figure 7. Even though O−PIII creates larger RMS surface roughness (2.43 nm) than N−PIII and C−PIII (see Figure 1S in the Supporting Information), the cytocompatibility is not superior. It is consistent with Yeung[27] et al.'s observation from PIII NiTi alloys. The performance of preosteoblasts and fibroblasts illustrates that a rough surface may enhance the cytocompatibility in vitro but does not appear to be the dominant factor. Other factors such as surface hydrophilicity and surface chemistry also need to be further considered.

Our results reveal that the surface hydrophilicity before and after PIII does not change significantly, and so the effect of surface hydrophilicity on the in vitro cytocompatibility can be neglected. On the other hand, the surface chemistry after C−PIII and N−PIII is altered dramatically and its effect on the cell behavior is quite prominent.[28] Moreover, small amounts of foreign atoms or molecules on the surface can dramatically alter the surface reactivity or performance of biomaterials. Previous studies suggest that the formation of TiN and TiC may impose positive effects on the cellular response[29,30] The cellular response involves a chain of complex biological reactions including protein adsorption, receptor−ligand binding, and signal transduction.[23] TiN can effectively stimulate cells to synthesize, secrete, and assemble the extracellular matrix (ECM) on the material surfaces.[31] The ECM is crucial to mediating cell adhesion onto biomaterials and its organization and production modulate cell attachment,[32] whereas the stimulation by TiC is usually manifested as enhanced gene expression associated with cell differentiation.[33] Hence, the biocompatible TiN and TiC layers stimulate preosteoblast and fibroblast response in the early stage of cell-material interaction.

Unintentional surface oxidation is observed after N−PIII and C−PIII and so the effects of surface oxidation on the cytocompatibility need to be considered as well. According to our data, the cytocompatibility on the O−PIII sample is only slightly higher than that on the unimplanted control but inferior to that on the N−PIII and C−PIII samples. Because O−PIII leads to more substantial surface oxidation than N−PIII or C−PIII, the contribution of surface oxidation to the cytocompatibility enhancement is inferred to be limited and there is evidence that the TiN and TiC play very important roles in the cytocompatibility enhancement in vitro.

The cytocompatibility is also closely related to corrosion resistance. The TiN and TiC layers being robust ceramic materials endow the Ti alloy with better corrosion resistance. It implies that they not only offer a relatively stable environment for cell adhesion and growth but also screen metal ions from the external environment, inhibit leaching of metal ions, and lead to reduced cytotoxicity.[34] However, the corrosion resistance is not the dominant factor determining cytocompatibility, because many types of corrosion-resistant materials are not biocompatible. According to our data and analysis, the cytocompatibility enhancement arises from the synergistic effects of the surface chemistry, surface roughness, and corrosion resistance. However, because the various surface characteristics of biomaterials are inter-related, it is difficult to isolate unequivocally their individual impact on the cytocompatibility.[22] Nonetheless, by comparing the two PIII processes, N−PIII more effectively promotes the functions of preosteoblasts and fibroblasts and it can be attributed to the TiN structure.

An important objective of this work is to improve the bone-forming ability and promote osseointegration. In the in vivo study, new bone formation and the bone−Ti interface are studied and the effects are quantified using microcomputed tomography. The results show that the N−PIII Ti pin induces the most substantial new bone formation and least bone resorption, followed by the C−PIII sample. The unimplanted control fares the worst. It should be noted that different from the conditions in vitro, a rough surface morphology appears to play a more significant role in bone growth in vivo because initial stability is more likely to be achieved on implants with a rough surface. A rough surface is also important to the establishment of a strong and long lasting connection between the implant and bone.[35,36] In particular, N−PIII yields a rough surface for cell adhesion and proliferation and coupled with the cytocompatible and corrosion-resistant TiN layer, the enhancement is most obvious and translates to osteoblast proliferation. Last but not least, no inflammation or necrosis is observed from the PIII samples, further demonstrating the nontoxicity of the materials and safe application in vivo.

5. CONCLUSION

Nitrogen and carbon plasma immersion ion implantation (PIII) is employed to modify Ti-6Al-4V alloy. Both processes promote cell adhesion and proliferation in vitro as well as new bone formation in vivo. The enhancement is attributed to the combined effects of the cytocompatibility, corrosion resistance, and surface roughness of the graded TiN and TiC surface structures produced by PIII. The effects of surface chemistry on the cytocompatibility are most dominant in vitro, whereas the increased surface roughness as a result of energetic ion bombardment may play a more important role in new bone formation in vivo. Compared to C−PIII, N−PIII is more effective and plasma-modified Ti-6Al-4V is safe to use clinically.

■ ASSOCIATED CONTENT

Supporting Information

AFM image of O−PIII Ti alloy (Figure S1); preosteoblasts and fibroblasts adhesion and proliferation on the O−PIII samples (Figure S2). This material is available free of charge via the Internet at http://pubs.acs.org/.

■ AUTHOR INFORMATION

Corresponding Author

*E-mail: wkkyeung@hku.hk (K.W.K.Y.); paul.chu@cityu.edu.hk (P.K.C.).

Notes

The authors declare no competing financial interest.

■ ACKNOWLEDGMENTS

This work was jointly supported by HKU Seed Funding for Basic Research, Hong Kong Research Grant Council General Reseasrch Fund 718507, 719411, 123708, 112510, and 112212, as well as City University of Hong Kong Applied Research Grant (ARG) #9667066.

■ REFERENCES

(1) Geetha, M.; Singh, A. K.; Asokamani, R.; Gogia, A. K. *Prog. Mater. Sci.* **2009**, *54*, 397−425.
(2) Hench, L. L.; Polak, J. M. *Science* **2002**, *295*, 1014−1017.
(3) Liu, X. Y.; Chu, P. K.; Ding, C. X. *Mater. Sci. Eng., R* **2004**, *47*, 49−121.
(4) Wang, H. Y.; Xu, M.; Wu, Z. W.; Zhang, W.; Ji, J. H.; Chu, P. K. *ACS Appl. Mater. Interfaces* **2012**, *4*, 4380−4386.
(5) Chu, P. K.; Chen, J. Y.; Wang, L. P.; Huang, N. *Mater. Sci. Eng., R* **2002**, *36*, 143−206.
(6) Liu, X. Y.; Chu, P. K; Ding, C. X. *Mater. Sci. Eng., R* **2010**, *70*, 275−302.
(7) Wu, G. S.; Feng, K.; Shanaghi, A.; Zhao, Y.; Xu, R. Z.; Yuan, G. Y.; Chu, P. K. *Surf. Coat. Technol.* **2012**, *206*, 3186−3195.
(8) Liu, X. M; Wu, S. L.; Chan, Y. L.; Chu, P. K.; Chung, C. Y.; Chu, C. L.; Yeung, K. W. K.; Lu, W. W.; Cheung, K. M. C.; Luk, K. D. K. *J. Biomed. Mater. Res., Part A* **2007**, *82*, 469−478.
(9) Oñate, J. I.; Alonso, F.; García, A. *Thin Solid Films* **1998**, *317*, 471−416.
(10) Alonso, F.; Arizaga, A.; Quainton, S.; Ugarte, J. J.; Viviente, J. L.; Oñate, J. I. *Surf. Coat. Technol.* **1995**, *74*−*75*, 986−992.
(11) Mello, C. B.; Ueda, M.; Silva, M. M.; Reuther, H.; Pichon, L.; Lepienski, C. M. *Wear* **2009**, *267*, 867−873.
(12) Luo, Y.; Ge, S. *Tribol. Int.* **2009**, *42*, 1373−1379.
(13) Chu, P. K. *J. Vac. Sci. Technol. B* **2004**, *22*, 289−296.
(14) Chu, P. K.; Tang, B. Y.; Wang, L. P.; Wang, X. F.; Wang, S. Y.; Huang, N. *Rev. Sci. Instrum.* **2001**, *72*, 1660−1665.
(15) Kokubo, T.; Kim, H. M.; Kawashita, M. *Biomaterials* **2003**, *24*, 2161−2175.
(16) http://srdata.nist.gov/ accessed January 30, 2013
(17) Zhao, Y.; Wong, S. M.; Wong, H. M.; Pan, H. B.; Yeung, K. W. K.; Chu, P. K. *Surf. Coat. Technol.* **2013**, DOI: 10.1016/j.surfcoat.2012.08.053.
(18) Zhao, Y.; Wu, G. S.; Pan, H. B.; Yeung, K. W. K.; Chu, P. K. *Mater. Chem. Phys.* **2012**, *132*, 187−191.
(19) Xie, Y. T.; Liu, X. Y.; Huang, A. P.; Ding, C. X.; Chu, P. K. *Biomaterials* **2005**, *26*, 6129−6135.
(20) Eriksson, C.; Ohlson, K.; Richter, K.; Billerdahl, N.; Johansson, M.; Nygren, H. *J. Biomed. Mater. Res.* **2007**, *83A*, 1062−1069.
(21) Kunzler, T. P.; Drobek, T.; Schuler, M.; Spencer, N. D. *Biomaterials* **2007**, *28*, 2175−2182.
(22) Liu, X. M.; Lim, J. Y.; Donahue, H. J.; Dhurjati, R.; Mastro, A. M.; Vogler, E. A. *Biomaterials* **2007**, *28*, 4535−4550.
(23) Deligianni, D. D.; Katsala, N.; Ladas, S.; Sotiropoulou, D.; Amedee, J.; Missirlis, Y. F. *Biomaterials* **2001**, *22*, 1241−1251.
(24) Keller, J. C.; Stanford, C. M.; Wightman, J. P.; Draughn, R. A.; Zaharias, R. *J. Biomed. Mater. Res.* **1994**, *28*, 939−946.
(25) Schwartz, Z.; Olivares-Navarrete, R.; Wieland, M.; Cochran, D. L.; Boyan, B. D. *Biomaterials* **2009**, *30*, 3390−3396.
(26) Saito, T.; Hayashi, H.; Kameyama, T.; Hishida, M.; Nagai, K.; Teraoka, K. *Mater. Sci. Eng., C* **2010**, *30*, 1.
(27) Yeung, K. W. K.; Chan, R. Y. L.; Lam, K. O.; Wu, S. L.; Liu, X. M.; Chung, C. Y.; Chu, P. K.; Lu, W. W.; Chan, D.; Luk, K. D. K.; Chung, K. M. C. *Surf. Coat. Technol.* **2007**, *202*, 1247−1251.
(28) Anselme, K. *Biomaterials* **2000**, *21*, 667−681.
(29) Groessner-Schreiber, B.; Neubert, A.; Müller, W. D.; Hopp, M.; Griepentrog, M.; Lange, K. P. *J. Biomed. Mater. Res., Part A* **2003**, *64A*, 591−599.
(30) Yeung, K. W. K.; Chan, Y. L.; Lam, K. O.; Liu, X. M.; Wu, S. L.; Liu, X. Y.; Chung, C. Y.; Lu, W. W.; Chan, D.; Luk, K. D. K.; Chu, P. K.; Cheung, K. M. C. *Mater. Sci. Eng., C* **2008**, *28*, 454−459.
(31) Gordin, D. M.; Gloriant, T.; Chane-Pane, V.; Busardo, D.; Mitran, V.; Höche, D.; Vasilescu, C.; Drob, S. I.; Cimpean, A. *J. Mater. Sci: Mater. Med.* **2012**, *23*, 2953−2966.
(32) Jayaraman, M.; Meyer, U.; Bühner, M.; Joos, U.; Wiesmann, H. P. *Biomaterials* **2004**, *25*, 625−631.
(33) Brama, M.; Rhodes, N.; Hunt, J.; Ricci, A.; Teghil, R.; Migliaccio, S.; Rocca, C. D.; Leccisotti, S.; Lioi, A.; Scandurra, M.; Maria, G. D.; Ferro, D.; Pu, F.; Panzini, G.; Politi, L.; Scandurra, R. *Biomaterials* **2007**, *28*, 595−608.
(34) Zhao, Y.; Wu, G.; Jiang, J.; Wong, H. M.; Yeung, K. W. K.; Chu, P. K. *Corros. Sci.* **2012**, *59*, 360−365.
(35) Rønold, H. J.; Ellingsen, J. E. *Biomaterials* **2002**, *23*, 4211−4219.
(36) Liu, X. M.; Wu, S. L.; Yeung, K. W. K.; Chan, Y. L.; Hu, T.; Xu, Z. S.; Liu, X. Y.; Chung, J. C. Y.; Cheung, K. M. C.; Chu, P. K. *Biomaterials* **2011**, *32*, 330−338.